



UNIVERSITY OF
GLOUCESTERSHIRE

This is a peer-reviewed, post-print (final draft post-refereeing) version of the following published document:

Toms, Phillip ORCID logoORCID: <https://orcid.org/0000-0003-2149-046X> (2013) Optical dating. In: Quaternary History & Palaeolithic Archaeology in the Axe Valley at Broom, South West England. Oxbow, pp. 157-164. ISBN 978-1-84217-520-0

EPrint URI: <https://eprints.glos.ac.uk/id/eprint/3402>

Disclaimer

The University of Gloucestershire has obtained warranties from all depositors as to their title in the material deposited and as to their right to deposit such material.

The University of Gloucestershire makes no representation or warranties of commercial utility, title, or fitness for a particular purpose or any other warranty, express or implied in respect of any material deposited.

The University of Gloucestershire makes no representation that the use of the materials will not infringe any patent, copyright, trademark or other property or proprietary rights.

The University of Gloucestershire accepts no liability for any infringement of intellectual property rights in any material deposited but will remove such material from public view pending investigation in the event of an allegation of any such infringement.

PLEASE SCROLL DOWN FOR TEXT.

This is the unformatted text for the article appearing as a chapter in the following published book:

Toms, Phillip (2013). *Optical dating*. In: Quaternary History & Palaeolithic Archaeology in the Axe Valley at Broom, South West England. Oxbow 157-164. ISBN 978-1-84217-520-0

Published by Oxbow Books, and available from:

<http://www.oxbowbooks.com/oxbow/catalogsearch/result/?q=axe+valley+at+broom>

We recommend you cite the published (post-print) version.

The URL for the published version is

<http://www.oxbowbooks.com/oxbow/catalogsearch/result/?q=axe+valley+at+broom>

Disclaimer

The University of Gloucestershire has obtained warranties from all depositors as to their title in the material deposited and as to their right to deposit such material.

The University of Gloucestershire makes no representation or warranties of commercial utility, title, or fitness for a particular purpose or any other warranty, express or implied in respect of any material deposited.

The University of Gloucestershire makes no representation that the use of the materials will not infringe any patent, copyright, trademark or other property or proprietary rights.

The University of Gloucestershire accepts no liability for any infringement of intellectual property rights in any material deposited but will remove such material from public view pending investigation in the event of an allegation of any such infringement.

PLEASE SCROLL DOWN FOR TEXT

Chapter 6

Optical dating

6.1 Introduction

The utility of optical dating (Huntley et al., 1985) lies in its potential to directly, accurately and precisely date sedimentary events where most other chronometric methods falter owing to limitations of context, material, age range and/or calibration. An optical age estimate should directly date the point of sediment burial. There is an increasing body of independent evidence that verifies this relationship (Murray and Olley, 2002). For certain periods, the maximum precision of optical ages (c. 5%) can be comparable if not superior to that of other chronometric methods, including radiocarbon. The datable signal is typically associated with ubiquitous and durable natural mineral grains. Its datable range is considerable, from as little as 50 years to as much as 750 ka and possibly beyond (Murray and Olley, 2002; Wang et al., 2006). Although it is necessary to calibrate the time dependent signal, this process does not generate multiple age estimates resultant of calibration plateaux that can afflict radiocarbon dating of certain periods. Aitken (1998) and Bøtter-Jensen et al. (2003) offer a detailed review of optical dating.

The fundamental requirements of any dating technique are two-fold; a time dependent signal and knowledge of this signal's size at the event to be dated. In Optical dating, the chronometric signal (Optically Stimulated Luminescence, OSL) is reset through exposure to sunlight and/or raised temperature. The datable event is the removal of these agents (e.g. through burial). The signal then accumulates over time as a function of low level, natural radiation exposure emanating from surrounding sediment as α, β, γ particles and the cosmos as electrons and muons. The luminescence signal is equivalent to a dosimeter providing a measure of total dose absorption (D_e). This signal is converted to a chronometer by estimating the rate of absorption (D_r ; Fig. 1), so that

$$\text{Age (ka)} = \frac{\text{Mean Equivalent Dose (D}_e\text{; in Gy)}}{\text{Mean Dose Rate (D}_r\text{; in Gy.ka}^{-1}\text{)}}$$

Optical dating has been deployed to directly date Broom's sediment sequence, defining a minimum age for the earliest incorporated artefacts and thus of earliest hominin occupation in the surrounding area during the Lower Palaeolithic. Together with optical dating of sites at Kilmington and Chard, these ages offer the first chronometric insight to the Axe Valley formation. This chapter outlines the findings from Toms et al. (2005; 2008), from which full details of optical dating at these sites can be acquired.

6.2 Methodology

6.2.1 Sampling

A total of eighteen samples were collected from the Middle Beds and Upper Gravels at Broom (Fig. 2, Table 1); the Lower Gravels remained inaccessible during the sampling period. Fifteen samples were obtained from matrix-supported units, extracted within opaque tubing or as lithified blocks to preserve the light sensitive datable signal. A further three samples were acquired from clast-supported material, excavating sediment into a light-tight bag 2 hrs after sunset with the aim of harnessing the chronometric signal residing within interstitial sands. A further ten samples were obtained from matrix-supported material using opaque tubing at Kilmington and Chard (Table 1).

6.2.2 Preparation

This element focussed on the isolation of quartz in the fine silt (5-15 μm) or fine sand (90-180 μm) range. The utility of this mineral in optical dating lies in the stability of its datable signal over the mid to late Quaternary period, predicted through isothermal decay studies (e.g. Smith et al., 1990) and evidenced by optical age estimates concordant with independent chronological controls (e.g. Murray and Olley, 2002). To preserve the time dependent signal, preparation

was conducted under subdued red light. Following removal of sunlight exposed material, the samples were dried at 40°C and then subjected to acid (10% HCl) and alkali (15% H₂O₂) digestion to remove carbonate and organic components. Fine sand was obtained by sieving and fine silt by acetone sedimentation. The analytical fraction was selected on the basis of the greatest mass. Fine sand samples were immersed in 40% HF for 1 hr to etch away the α -irradiated rind and to degrade feldspars. 10% HCl was added to remove acid soluble fluorides. Samples were then resieved to remove feldspars and density separated at 2.68 g.cm⁻³ to segregate quartz from heavy minerals. Fine silt samples were placed in 35% H₂SiF₆ for 2 weeks (Jackson et al., 1976; Berger et al., 1980) and 10% HCl for 1 hr to digest all but quartz and a minor component of heavy minerals. Aliquots (1.5-5 mg) were mounted on 12 aluminium discs for luminescence measurement and calibration of each sample.

6.2.3 D_e measurement

All natural sedimentary minerals exhibit marked inter-grain variability in luminescence per unit dose. Owing to this variation in sensitivity, the estimation of D_e acquired since burial requires calibration of the natural signal using known amounts of laboratory dose. D_e values were quantified using a single-aliquot regenerative-dose (SAR) protocol, similar to that outlined by Murray and Wintle (2000). This process was facilitated by a Risø TL-DA-15 irradiation-stimulation-detection system (Markey et al., 1997). Optical signal stimulation was provided by a tungsten halogen lamp, filtered to broad blue-green light. Stimulation occurred whilst aliquots were held at 160°C (Broom only) or 125°C, principally to enhance the signal to noise ratio. Optically stimulated UV emissions from the quartz aliquots were detected by an EMI 9235QA photomultiplier. Aliquot irradiation was conducted using a calibrated 1.48 GBq ⁹⁰Sr/⁹⁰Y β source. The presence of contaminant feldspar grains was assessed through infrared stimulation (Hütt et al., 1988). Significant IR stimulated luminescence was detected from only GL06012, qualifying the presence of feldspars and thus for potential for anomalous fading of the time dependent signal in this sample (Wintle, 1973). SAR by definition evaluates D_e through measuring the natural signal (Fig. 3) of a single aliquot and then regenerating that aliquot's signal by using known laboratory doses to enable calibration. For each aliquot, up to 6 different regenerative-doses were administered so as to image dose response. D_e values for each aliquot were then interpolated, and associated counting and fitting errors calculated by way of exponential plus linear regression (Fig. 3). Preheating aliquots between irradiation and optical stimulation was necessary to ensure comparability between natural and laboratory-induced signals. Aliquots were preheated at 260°C for 10s prior to measurement of natural and regenerated signals. As a result of D_e preheat dependence and dose recovery tests, some samples from Kilmington and Chard were preheated at 240°C for 10s (Murray and Wintle, 2003; Toms et al., 2008). However, the multiple irradiation and preheating steps that are required to define single-aliquot regenerative-dose response leads to signal sensitisation, rendering calibration of the natural signal inaccurate. The SAR protocol (Murray and Wintle, 2000) enables this sensitisation between irradiation-preheat steps to be tracked and corrected using a test dose; set at 5 Gy preheated to 180°C (Broom only) or 220°C for 10s. The reliability of correction can be quantified by examining the reproducibility of corrected signals from repeat regenerative-doses. The majority of aliquots generated a repeat ratio statistically concordant with unity, verifying reliability of sensitisation correction. Weighted mean D_e values were calculated using the central age model outlined by Galbraith et al. (1999) and are quoted at 1 σ confidence (Table 1).

6.2.4 D_r measurement

Lithogenic D_r values were defined through measurement of U, Th and K radionuclide concentration and conversion of these quantities into α , β and γ D_r values (Table 1). α and β contributions were estimated from sub-samples by Neutron Activation Analysis (NAA) delivered by Becquerel Canada or, where low U (<0.1 ppm) and/or Th (<0.05 ppm) occurred, Inductively Coupled Plasma Mass Spectrometry (ICP-MS) delivered by the University of Oxford. γ dose rates were estimated from *in situ* gamma spectrometry or, where direct measurements were not possible, from NAA or ICP-MS of sub-samples. *In situ* measurements were conducted using an EG&G μ Nomad portable NaI gamma spectrometer (calibrated using the block standards at RLAHA, University of Oxford); these reduce uncertainty relating to potential

heterogeneity in the γ dose field surrounding each sample. For samples from Kilmington and Chard, laboratory-based γ spectrometry was conducted using an Ortec GEM-S high purity Ge coaxial detector system, calibrated using certified reference materials supplied by CANMET. These high resolution spectra revealed negligible U-series disequilibrium. Estimates of radionuclide concentration were converted into D_r values (Adamiec and Aitken, 1998), accounting for D_r modulation forced by grain size (Mejdahl, 1979), present moisture content (Zimmerman, 1971) and, where D_e values are generated from 5-15 μm quartz, reduced signal sensitivity to α radiation (a -value 0.050 ± 0.002 ; Toms, unpub. data). Cosmogenic D_r values are calculated on the basis of sample depth, geographical position and matrix density (Prescott and Hutton, 1994).

6.2.5 Age Calculation and Verification

The luminescence ages given in Table 1 are the quotient of mean D_e and D_r values, with associated 1σ uncertainties reflecting the propagation of systematic and experimental errors. The principal concern in respect of this study is the antiquity of the age estimates. Matters of signal saturation and retention, both leading to age underestimation, are of relevance. There is limited precedent by which to adjudge accuracy through extrapolation from previous studies. Murray et al. (2002) demonstrated that mean D_e estimates corresponding with high-doses of 200-400 Gy generated ages consistent with the last Interglacial and concordant with independent chronological control. Watanuki et al. (2005) independently verified optical age estimates back to 500 ka for a Japanese loess sequence. At the level of the Bruhnes-Matuyama boundary within the Chinese loess-palaeosol sequence, Wang et al. (2006) achieved an optical age coeval with the timing of this switch from reversed to normal magnetic polarity at c. 775 ka. However, given that these examples represent the near breadth of independently verified, Middle Pleistocene quartz optical age estimates, it is preferable to adopt the same approach as these studies rather than extrapolate from them. The caveat is that the Axe Valley formation has no chronological controls by which to corroborate the optical ages presented here. Despite this dearth of extrinsic verification, there exists a credible intrinsic gauge. Convergent age estimates from stratigraphically equivalent positions of divergent D_r values provide a simple, yet powerful intrinsic index of reliability (Toms et al., 2005). Such relationships supersede concerns of inaccuracy potentially forced by any one of the variables associated with D_e and D_r but whose influence can be difficult to assess. This fundamental approach requires multiple samples be obtained from equivalent stratigraphic units, targeting areas of divergent dosimetry. $D_r:D_e$ plots (Toms et al., 2005) then readily illustrate the occurrence of linear relationships, as well as rapidly communicate the spread of ages within a study (Figs. 4 and 5). This assessment of accuracy can be supplemented by Bayesian modelling. Coupling absolute age estimates with knowledge of their relative stratigraphic position can quantify the stratigraphic consistency and refine the precision of the optical chronology. Bayesian analysis of Broom's optical ages is presented in Fig. 6.

6.3 Results and Discussion

The spread of age estimates is illustrated in Figs. 4 and 5 and data detailed in Table 1. At Broom, it is apparent that GL03057 to GL03059 (section 14) are significantly younger than all other age estimates and are indeed younger than the Middle Pleistocene age inferred from the site's Lower Palaeolithic assemblage. These younger estimates likely reflect reworked material, possibly resulting from 20th century quarrying. Interstitial sand samples obtained from clast-supported material (GL03001 to GL03003, section 9) are considerably older than matrix-supported samples. These extreme ages could be a function of partial resetting of the pre-burial signal, incorporation of post-depositionally formed fragments of chert and flint within aliquots and/or an underestimation of D_r . These non-conventional samples are the subject of further study. Incorporating uncertainties, age estimates from matrix-supported material other than that in section 14 span 209 to 317 ka for the Upper Gravels and 259 to 326 ka for the Middle Beds. Within Fig. 4 isochrons are fitted to data from the Middle Beds and Upper Gravels, discounting that from section 14 and the upper unit of section 9 for the reasons given above. At 1σ confidence, 67% of age estimates are concordant with their respective isochron, at 2σ , 92% are consistent.

The significant difference between lower and upper D_r values from each unit and broad statistical consistency of $D_r:D_e$ data with their respective isochron suggests a reasonable level of reliability.

All but one sample (GL06001) from Kilmington and Chard generated age estimates consistent with their relative stratigraphic position at each site. GL06001 may have been obtained from a slipped deposit that is in effect stratigraphically younger than samples from the lower units. At Kilmington, the deposits span 135 to 336 ka, whilst those at Chard range between 86 and 401 ka. Fig. 5 shows $D_e:D_r$ plots from Kilmington and Chard, illustrating the spread of luminescence ages and demonstrating the reliability of the ages from the upper unit where a significant variation in D_r was recorded, yet coeval estimates of age were generated.

Fig. 6 details the Bayesian output from Oxcal v3.5 (Bronk Ramsey, 1995; 2001) for the Middle Beds and Upper Gravels at Broom based on the optical age and relative stratigraphic position of each sample. Within Bayesian modelling of sedimentary succession, phases refer to age estimates forming part of a sedimentary sequence yet without an explicit definition of their relative stratigraphic position. Sequences consist of age estimates and/or phases whose relative stratigraphic position is known. Age estimates from the Middle Beds were all obtained from section 2 and were therefore defined sequentially as their relative stratigraphic position was unambiguous. The Upper Gravels comprise age estimates from multiple sections. These sections consist of either a single age estimate (e.g. section 1) or multiple estimates for which relative stratigraphic position is known (e.g. section 13). Some complexity exists at section 9; the sand unit has three observable horizons into which optical age estimates can be grouped, however their relative position within these horizons is ambiguous. Hence, whilst horizons are defined as a sequence, age estimates within each are defined as a phase. Age estimates within the Upper Gravels from multiple sections can be considered as forming part of an Upper Gravel phase. Bronk Ramsey (1995) suggests an overall agreement index (A) of 60% as a rejection threshold for a series of ages. The A value of c. 102% given in Fig. 5 suggests the optical chronology is consistent with the relative stratigraphic position of the Middle Beds and Upper Gravels. Further, this modelled data theorises improved estimates of precision. At 1σ confidence the optical chronology is refined to Middle Bed formation between 324 and 282 ka and Upper Gravels between 292 and 205 ka.

From these data, the Lower Gravels formed either before or during the early part of the Marine Isotope Stage (MIS) 9 interglacial, the Middle Beds between mid MIS 9 and early MIS 8 (glacial) and the Upper Gravels during MIS 8 and MIS 7 (interglacial). The general synchrony of incision and accumulation of coarse deposits with cool conditions and fines with warm conditions broadly typifies the model of fluvial terrace formation (Bridgland, 2000). However, the continued accumulation of Upper Gravels into the interglacial of MIS 7 runs counter to this model.

6.4 Conclusions

Optical dating suggests deposition of the proto Axe is recorded between 86 and 401 ka (MIS 5 to 10). Fluvial sedimentation at Broom appears to have been focussed between 209 and 326 ka (MIS 7 to 9). By inference, the undated Lower Gravels at Broom containing the first appearance of artefacts at this site suggest the earliest hominin presence likely occurred prior to 326 ka, possibly before or in the early part of the interglacial of MIS 9. These age estimates for elements of the Axe Valley Formation are amongst the oldest optical dates published for UK deposits. The apparent internal and stratigraphic consistency of the optical chronology, in particular at Broom, is encouraging. However, the discrepancy in minimum age reported for the Upper Gravels at Broom with that extrapolated from Bridgland's (2000) model of terrace evolution highlights the tentative nature of a Mid-Pleistocene optical chronology.

References

- Adamiec, G. and Aitken, M. J. (1998) Dose-rate conversion factors: new data. *Ancient TL*, 16, 37-50.
- Aitken, M. J. (1998) An introduction to optical dating: the dating of Quaternary sediments by the use of photon-stimulated luminescence. Oxford University Press.
- Berger, G. W., Mulhern, P. J. and Huntley, D. J. (1980). Isolation of silt-sized quartz from sediments. *Ancient TL*, 11, 147-152.
- Bøtter-Jensen, L., McKeever, S. W. S. and Wintle, A. G. (2003) *Optically Stimulated Luminescence Dosimetry*. Elsevier, Amsterdam.
- Bridgland, D. R. (2000) River terrace systems in north-west Europe: an archive of environmental change, uplift and early human occupation. *Quaternary Science Reviews*, 19, 1293–1303.
- Bronk Ramsey, C. (1995) Radiocarbon calibration and analysis of stratigraphy: The OxCal program. *Radiocarbon*, 37, 425-430.
- Bronk Ramsey, C. (2001) Development of the Radiocarbon Program OxCal. *Radiocarbon*, 43, 355-363.
- Galbraith, R. F., Roberts, R. G., Laslett, G. M., Yoshida, H. and Olley, J. M. (1999) Optical dating of single and multiple grains of quartz from Jinmium rock shelter (northern Australia): Part I, Experimental design and statistical models. *Archaeometry*, 41, 339-364.
- Huntley, D. J., Godfrey-Smith, D. I. and Thewalt, M. L. W. (1985) Optical dating of sediments. *Nature*, 313, 105-107.
- Hütt, G., Jaek, I. and Tchonka, J. (1988) Optical dating: K-feldspars optical response stimulation spectra. *Quaternary Science Reviews*, 7, 381-386.
- Jackson, M. L., Sayin, M. and Clayton, R. N. (1976) Hexafluorosilicic acid reagent modification for quartz isolation. *Soil Science Society of America Journal*, 40, 958-960.
- Markey, B. G., Bøtter-Jensen, L., and Duller, G. A. T. (1997) A new flexible system for measuring thermally and optically stimulated luminescence. *Radiation Measurements*, 27, 83-89.
- Mejdahl, V. (1979) Thermoluminescence dating: beta-dose attenuation in quartz grains. *Archaeometry*, 21, 61-72.
- Murray, A. S. and Olley, J. M. (2002) Precision and accuracy in the Optically Stimulated Luminescence dating of sedimentary quartz: a status review. *Geochronometria*, 21, 1-16.
- Murray, A. S. and Wintle, A. G. (2000) Luminescence dating of quartz using an improved single-aliquot regenerative-dose protocol. *Radiation Measurements*, 32, 57-73.
- Murray, A. S. and Wintle, A. G. (2003) The single aliquot regenerative dose protocol: potential for improvements in reliability. *Radiation Measurements*, 37, 377-381.

- Murray, A. S., Wintle, A. G., and Wallinga, J. (2002) Dose estimation using quartz OSL in the non-linear region of the growth curve. *Radiation Protection Dosimetry*, **101**, 371-374.
- Prescott, J. R. and Hutton, J. T. (1994) Cosmic ray contributions to dose rates for luminescence and ESR dating: large depths and long-term time variations. *Radiation Measurements*, **23**, 497-500.
- Smith, B. W., Rhodes, E. J., Stokes, S., Spooner, N. A. (1990) The optical dating of sediments using quartz. *Radiation Protection Dosimetry*, **34**, 75-78.
- Toms, P. S., Hosfield, R. T., Chambers, J. C., Green, C. P. and Marshall, P. (2005) Optical dating of the Broom Palaeolithic sites, Devon and Dorset. English Heritage Centre for Archaeology Report 16/2005.
- Toms, P. S., Brown, A. G., Basell, L. S., and Hosfield, R. T. (2008) Palaeolithic Rivers of South-West Britain: optically stimulated luminescence dating of residual deposits of the proto-Axe, Exe, Otter, and Washford, English Heritage Research Department Report Series 2/2008.
- Wang, X. L., Lu, Y. C. and Wintle, A. G. (2006) Recuperated OSL dating of fine-grained quartz in Chinese loess. *Quaternary Geochronology*, **1**, 89-100.
- Watanuki, T., Murray, A. S. and Tsukamoto, S. (2005) Quartz and polymineral luminescence dating of Japanese loess over the last 0.6 Ma: Comparison with an independent chronology. *Earth and Planetary Science Letters*, **240**, 774-789.
- Wintle, A. G. (1973) Anomalous fading of thermoluminescence in mineral samples. *Nature*, **245**, 143-144.
- Zimmerman, D. W. (1971) Thermoluminescent dating using fine grains from pottery. *Archaeometry*, **13**, 29-52.

Laboratory Code	Depth (m)	Grain size (μm)	Moisture content	Nal γ -spectrometry (in situ)			γ D _r (Gy.ka ⁻¹)	Neutron Activation Analysis (¹⁰ Or ICP-MS)			α D _r (Gy.ka ⁻¹)	β D _r (Gy.ka ⁻¹)	Cosmic D _r ² (Gy.ka ⁻¹)	Total D _r (Gy.ka ⁻¹)	D _e (Gy)	Age (ka)
				K (%)	Th (ppm)	U (ppm)		K (%)	Th (ppm)	U (ppm)						
				Broom												
GL02082	5.10	90-125	0.18 ± 0.05	0.72 ± 0.02	6.82 ± 0.22	1.60 ± 0.09	0.54 ± 0.04	1.11 ± 0.06	9.68 ± 0.48	2.41 ± 0.12	-	1.08 ± 0.10	0.09 ± 0.01	1.72 ± 0.11	503.4 ± 27.8	293 ± 24
GL02083	15.60	125-180	0.17 ± 0.04	1.11 ± 0.02	7.78 ± 0.24	2.48 ± 0.11	0.75 ± 0.06	0.81 ± 0.04	7.32 ± 0.37	1.99 ± 0.10	-	0.81 ± 0.07	0.05 ± 0.00	1.61 ± 0.08	461.5 ± 28.0	287 ± 22
GL02084	16.50	90-125	0.17 ± 0.04	1.15 ± 0.02	7.15 ± 0.21	2.15 ± 0.10	0.70 ± 0.05	1.10 ± 0.06	6.86 ± 0.34	1.90 ± 0.10	-	0.98 ± 0.09	0.05 ± 0.00	1.73 ± 0.10	483.0 ± 21.0	279 ± 20
GL02085	2.78	125-180	0.18 ± 0.04	0.85 ± 0.02	4.63 ± 0.19	0.90 ± 0.08	0.42 ± 0.03	0.96 ± 0.05	4.28 ± 0.21	0.80 ± 0.04	-	0.71 ± 0.07	0.13 ± 0.01	1.27 ± 0.08	353.4 ± 21.4	279 ± 24
GL03001 ¹	1.65	125-180	0.07 ± 0.02	0.15 ± 0.01	1.64 ± 0.10	0.85 ± 0.07	0.19 ± 0.02	0.19 ± 0.01	2.44 ± 0.08	0.58 ± 0.03	-	0.24 ± 0.02	0.16 ± 0.02	0.60 ± 0.03	274.3 ± 18.5	460 ± 38
GL03002 ¹¹	2.12	125-180	0.10 ± 0.03	-	-	-	0.16 ± 0.02	0.17 ± 0.01	1.80 ± 0.07	0.45 ± 0.02	-	0.19 ± 0.02	0.15 ± 0.02	0.50 ± 0.03	367.8 ± 39.0	739 ± 89
GL03003 ¹	2.68	125-180	0.11 ± 0.03	0.17 ± 0.01	1.75 ± 0.11	0.87 ± 0.07	0.20 ± 0.02	0.15 ± 0.01	1.17 ± 0.03	0.58 ± 0.02	-	0.19 ± 0.02	0.13 ± 0.01	0.52 ± 0.02	449.8 ± 33.3	870 ± 76
GL03004	2.66	125-180	0.11 ± 0.03	0.45 ± 0.01	2.85 ± 0.13	1.20 ± 0.08	0.33 ± 0.03	0.73 ± 0.04	4.40 ± 0.22	0.51 ± 0.03	-	0.61 ± 0.05	0.13 ± 0.01	1.08 ± 0.05	288.3 ± 19.1	268 ± 22
GL03005	2.95	125-180	0.14 ± 0.03	0.60 ± 0.02	4.56 ± 0.16	2.17 ± 0.11	0.52 ± 0.04	0.89 ± 0.04	6.96 ± 0.35	1.14 ± 0.06	-	0.80 ± 0.07	0.13 ± 0.01	1.45 ± 0.07	326.8 ± 17.3	226 ± 16
GL03006	2.81	125-180	0.14 ± 0.03	0.57 ± 0.02	3.45 ± 0.15	1.45 ± 0.09	0.40 ± 0.03	0.99 ± 0.05	5.80 ± 0.29	1.02 ± 0.05	-	0.83 ± 0.07	0.13 ± 0.01	1.36 ± 0.08	375.9 ± 27.1	277 ± 25
GL03007	2.96	125-180	0.13 ± 0.03	0.66 ± 0.02	4.10 ± 0.17	1.12 ± 0.10	0.41 ± 0.04	0.83 ± 0.04	4.24 ± 0.21	0.48 ± 0.02	-	0.65 ± 0.06	0.13 ± 0.01	1.19 ± 0.06	324.0 ± 20.8	271 ± 22
GL03008	0.95	125-180	0.14 ± 0.04	0.84 ± 0.02	4.53 ± 0.16	1.98 ± 0.10	0.54 ± 0.04	0.88 ± 0.04	4.47 ± 0.22	0.99 ± 0.05	-	0.73 ± 0.07	0.18 ± 0.03	1.45 ± 0.07	352.8 ± 18.9	244 ± 18
GL03009	1.09	125-180	0.14 ± 0.03	0.57 ± 0.02	4.10 ± 0.17	1.95 ± 0.11	0.47 ± 0.04	0.64 ± 0.03	5.53 ± 0.28	1.26 ± 0.06	-	0.63 ± 0.05	0.17 ± 0.02	1.27 ± 0.06	343.0 ± 18.6	270 ± 19
GL03010 ¹¹	15.00	125-180	0.18 ± 0.05	-	-	-	0.67 ± 0.07	0.94 ± 0.05	7.66 ± 0.38	2.22 ± 0.11	-	0.90 ± 0.09	0.03 ± 0.00	1.61 ± 0.12	380.6 ± 28.0	237 ± 25
GL03011	16.20	125-180	0.17 ± 0.04	0.95 ± 0.03	7.29 ± 0.27	3.98 ± 0.18	0.83 ± 0.08	1.02 ± 0.05	8.25 ± 0.41	2.24 ± 0.11	-	0.98 ± 0.09	0.03 ± 0.00	1.84 ± 0.10	546.0 ± 44.8	297 ± 29
GL03057	10.43	5-15	0.27 ± 0.07	1.14 ± 0.03	9.06 ± 0.31	2.82 ± 0.19	0.72 ± 0.08	1.19 ± 0.06	6.90 ± 0.35	1.98 ± 0.10	0.27 ± 0.04	0.96 ± 0.11	0.05 ± 0.00	2.01 ± 0.12	39.8 ± 1.7	24 ± 2
GL03058	10.65	5-15	0.29 ± 0.07	1.23 ± 0.04	9.12 ± 0.31	3.38 ± 0.20	0.76 ± 0.09	1.62 ± 0.08	13.60 ± 0.68	1.92 ± 0.10	0.39 ± 0.05	1.27 ± 0.16	0.05 ± 0.00	2.47 ± 0.17	39.6 ± 2.7	20 ± 2
GL03059	10.81	5-15	0.25 ± 0.06	1.27 ± 0.03	8.46 ± 0.29	3.11 ± 0.18	0.77 ± 0.08	1.22 ± 0.06	6.39 ± 0.32	1.30 ± 0.07	0.22 ± 0.03	0.93 ± 0.10	0.05 ± 0.00	1.98 ± 0.11	57.5 ± 3.6	34 ± 2
Kilmington																
GL06001	5.0	125-180	0.18 ± 0.05	0.49 ± 0.02	3.73 ± 0.13	1.69 ± 0.09	0.49 ± 0.02	2.10 ± 0.09	10.26 ± 0.44	2.85 ± 0.14	-	1.68 ± 0.17	0.10 ± 0.01	2.27 ± 0.17	350.2 ± 35.8	154 ± 19
GL06002	5.0	125-180	0.16 ± 0.04	0.51 ± 0.01	2.83 ± 0.12	1.10 ± 0.07	0.38 ± 0.02	1.33 ± 0.06	6.14 ± 0.27	1.56 ± 0.09	-	1.08 ± 0.10	0.10 ± 0.01	1.55 ± 0.10	480.5 ± 26.6	309 ± 26
GL06003	2.0	125-180	0.14 ± 0.03	0.57 ± 0.02	3.49 ± 0.16	1.20 ± 0.10	0.44 ± 0.02	1.52 ± 0.07	8.62 ± 0.37	2.42 ± 0.12	-	1.36 ± 0.11	0.15 ± 0.01	1.95 ± 0.12	348.7 ± 28.3	179 ± 18
GL06004	4.0	125-180	0.06 ± 0.01	0.38 ± 0.02	1.85 ± 0.13	0.87 ± 0.09	0.28 ± 0.01	0.62 ± 0.03	2.07 ± 0.11	0.52 ± 0.04	-	0.53 ± 0.04	0.11 ± 0.01	0.92 ± 0.04	250.6 ± 20.5	273 ± 26
Chard																
GL06010	4.3	125-180	0.16 ± 0.04	0.36 ± 0.01	2.28 ± 0.12	1.29 ± 0.08	0.34 ± 0.02	1.27 ± 0.06	6.86 ± 0.29	2.08 ± 0.10	-	1.09 ± 0.10	0.11 ± 0.01	1.54 ± 0.10	268.5 ± 22.0	174 ± 18
GL06011	2.5	125-180	0.13 ± 0.03	0.30 ± 0.01	2.12 ± 0.10	1.01 ± 0.07	0.29 ± 0.01	0.60 ± 0.03	3.10 ± 0.15	0.95 ± 0.06	-	0.53 ± 0.04	0.14 ± 0.01	0.96 ± 0.05	90.2 ± 6.8	94 ± 9
GL06012	1.7	125-180	0.14 ± 0.03	0.68 ± 0.02	3.85 ± 0.17	1.62 ± 0.11	0.53 ± 0.02	1.53 ± 0.07	7.23 ± 0.31	1.90 ± 0.09	-	1.28 ± 0.11	0.16 ± 0.02	1.97 ± 0.11	193.7 ± 11.0	98 ± 9
GL06013	4.5	125-180	0.15 ± 0.04	0.36 ± 0.02	1.82 ± 0.13	0.79 ± 0.08	0.26 ± 0.01	0.99 ± 0.05	2.71 ± 0.13	0.65 ± 0.05	-	0.72 ± 0.07	0.10 ± 0.01	1.09 ± 0.07	298.6 ± 19.2	274 ± 25
GL06057	6.7	125-180	0.16 ± 0.04	0.18 ± 0.01	1.32 ± 0.08	0.82 ± 0.06	0.20 ± 0.01	0.87 ± 0.04	5.30 ± 0.21	1.30 ± 0.05	-	0.75 ± 0.07	0.08 ± 0.01	1.02 ± 0.07	375.3 ± 24.6	367 ± 35
GL06058	7.0	125-180	0.15 ± 0.04	0.23 ± 0.01	1.55 ± 0.10	0.67 ± 0.07	0.21 ± 0.01	1.09 ± 0.05	3.90 ± 0.16	1.00 ± 0.04	-	0.84 ± 0.08	0.07 ± 0.01	1.12 ± 0.08	318.3 ± 33.3	284 ± 36

¹ γ dose rate calculated using radionuclide concentrations determined from ICP-MS assay of combined sub-samples

² Sites located at approximately 51°N, 3°W; Broom, 50 m asl; Chard, 80 m asl; Kilmington, 40 m asl

Table 1 Dosimetry, D_e and age data obtained by multi-grain single-aliquot optical dating of Broom, Kilmington and Chard.

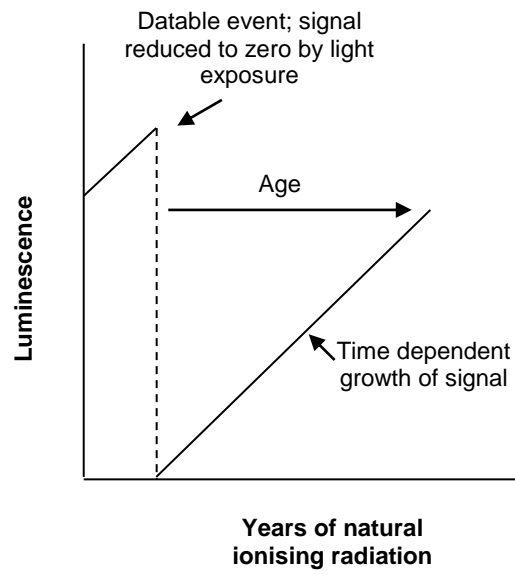


Fig. 1 Basic principles of optical dating

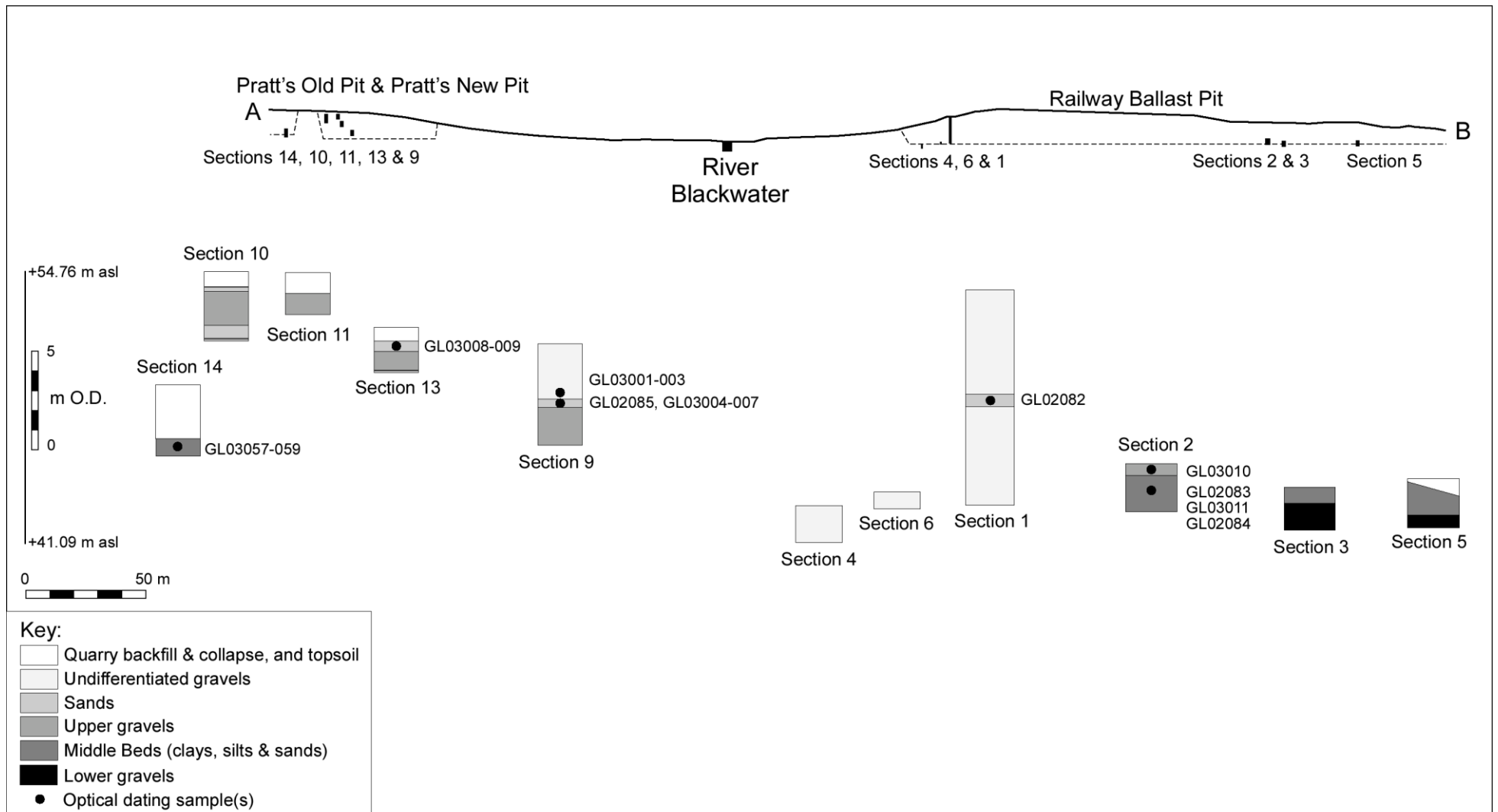


Fig. 2 Schematic of stratigraphy of the Broom deposits and position of optical dating samples (listed in descending stratigraphic order).

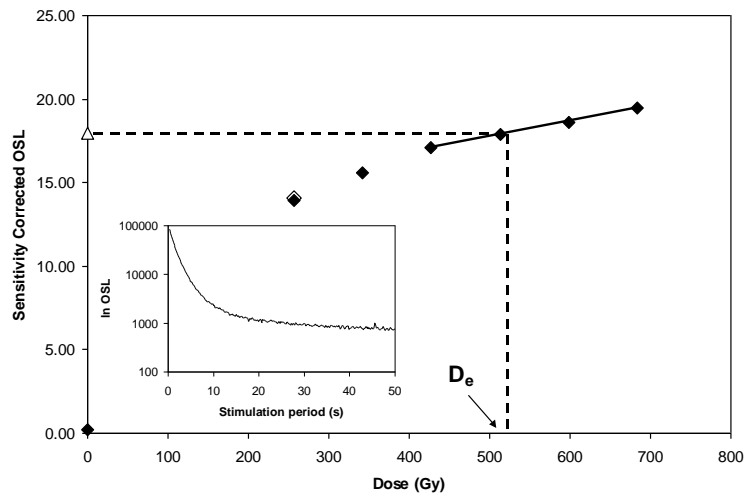


Fig. 3 Aliquot 1 sample GL03011, an example of natural optical signal from a multi-grain quartz aliquot (*inset*) and of sensitivity corrected optical response to high doses. The interpolated D_e value is indicated, the natural signal is denoted by an open triangle, regenerative-dose signals by filled diamonds and repeat regenerative-dose response by an open diamond.

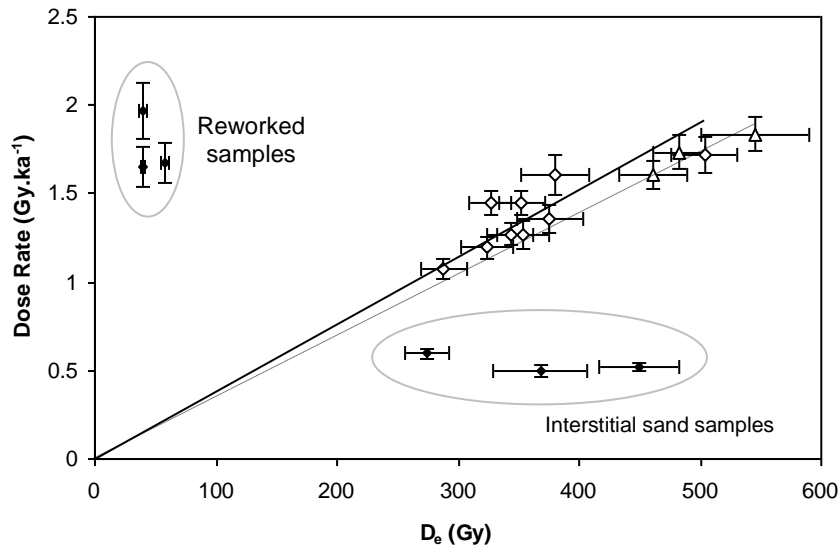


Fig. 4 Bivariation of age parameters for samples from the Middle Beds (open triangles), Upper Gravels (open diamonds) and rejected age estimates (filled diamonds). The gradient of lines drawn from the origin to the data point of each sample is the reciprocal of sample age; the shallower the gradient, the older the age estimate. Reworked samples and non-conventional interstitial sand samples are highlighted. The curves shown are fitted to data derived from conventional, matrix-supported samples from the Middle Beds (dashed) and Upper Gravels (solid).

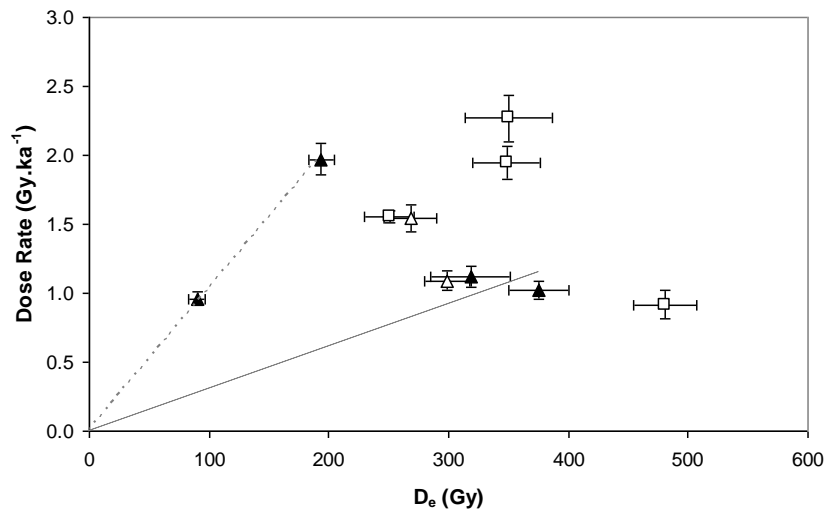


Fig. 5 Bivariation of age parameters for samples from Kilmington (squares) and Chard (triangles). Isochrons are fitted to data derived from samples taken from equivalent stratigraphic units (filled symbols).

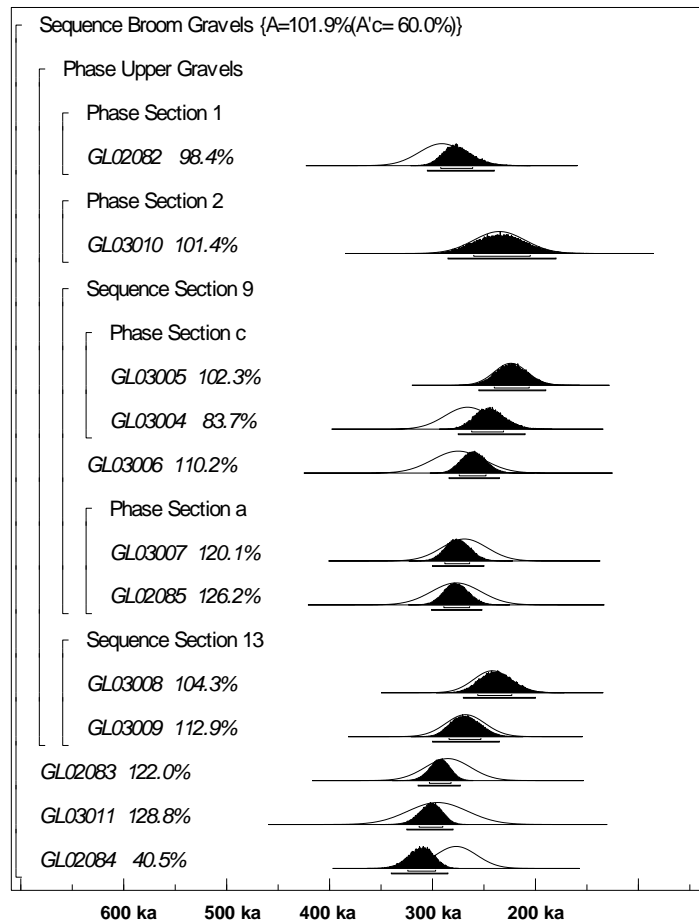


Fig. 6 Bayesian modelling of accepted optical age estimates within the Middle Beds and Upper Gravels. Filled distributions reflect the probability distributions of raw optical age estimates, unfilled represent modelled distributions. Agreement indices for each sample are shown next to each sample code. The overall agreement index (A_{overall}) quantifies the consistency of age estimates with their relative stratigraphic position; $A_{\text{overall}} = 60\%$ is the rejection threshold for a series of dates. See text for further details.